



**HAL**  
open science

## Power exchanged between subsystems with non-diffuse fields in statistical energy analysis

V. Tyrode, N. Totaro, Laurent Maxit, A. Le Bot

### ► To cite this version:

V. Tyrode, N. Totaro, Laurent Maxit, A. Le Bot. Power exchanged between subsystems with non-diffuse fields in statistical energy analysis. *Journal of the Acoustical Society of America*, 2023, 153 (5), pp.3036. 10.1121/10.0019551 . hal-04113016

**HAL Id: hal-04113016**

**<https://hal.science/hal-04113016v1>**

Submitted on 15 May 2024

**HAL** is a multi-disciplinary open access archive for the deposit and dissemination of scientific research documents, whether they are published or not. The documents may come from teaching and research institutions in France or abroad, or from public or private research centers.

L'archive ouverte pluridisciplinaire **HAL**, est destinée au dépôt et à la diffusion de documents scientifiques de niveau recherche, publiés ou non, émanant des établissements d'enseignement et de recherche français ou étrangers, des laboratoires publics ou privés.

# Power exchanged between subsystems with non-diffuse fields in statistical energy analysis.

V. Tyrode,<sup>1</sup> N. Totaro,<sup>2</sup> L. Maxit,<sup>2</sup> and A. Le Bot<sup>1, a</sup>

<sup>1</sup>*Univ Lyon, Ecole Centrale de Lyon, Laboratory of tribology and system dynamics, UMR CNRS 5513, 69134, Ecully, France*

<sup>2</sup>*Univ Lyon, INSA Lyon, LVA, EA677, 69621 Villeurbanne, France*

(Dated: 25 April 2023)

1 This article is a discussion on the necessity of the assumption of diffuse field in sta-  
2 tistical energy analysis (SEA) and the validity of the coupling power proportionality  
3 which states that the vibrational power exchanged between coupled subsystems is  
4 proportional to the difference of their modal energies. It is proposed to re-formulate  
5 the coupling power proportionality in terms of *local energy density* instead of *modal*  
6 *energy*. We show that this generalized form remains valid even if the vibrational field  
7 is not diffuse. Three causes of lack of diffuseness have been studied: coherence of rays  
8 in symmetrical geometries, non ergodic geometries, and the effect of high damping.  
9 Numerical simulations and experimental results conducted on flat plates in flexural  
10 vibration are provided to support these statements.

---

<sup>a</sup>alain.le-bot@ec-lyon.fr

## 11 I. INTRODUCTION

12 Predicting the dynamical behaviour of structures in the low frequency range is a problem  
13 that is largely overcome today. But at high frequencies, the classical methods like the well-  
14 known finite element analysis become quickly inefficient. This has motivated the emergence  
15 of methods with a lower numerical cost like statistical energy analysis (SEA)<sup>1-4</sup> (see Ref.<sup>5</sup>  
16 for an up-to-date synthesis of the theory).

17 The principle of SEA is to subdivide a complex system into subsystems and to analyze  
18 their exchanges of vibrational energy. The main result which allows a systemic approach is  
19 the so-called *coupling power proportionality* which claims that the power exchanged between  
20 two lightly coupled subsystems is proportional to the difference of their modal energies also  
21 referred to as vibrational temperatures. It is in this way that SEA may be interpreted as  
22 the theory of thermodynamics of sound and vibration<sup>6</sup>.

23 The foundation of the coupling power proportionality must be found in the assumption  
24 of modal energy equipartition, or equivalently, in the assumption of diffuse field (see Refs.<sup>7,8</sup>  
25 for a definition of diffuse field). Several alternative theories have been proposed to relax  
26 these assumptions. The theory of statistical energy modal distribution analysis (SmEdA)<sup>9,10</sup>  
27 extends SEA to mid-frequencies by setting power balance equations to individual modes  
28 instead of mode packets making it possible not to assume energy equipartition. Whereas  
29 non-diffuse fields are naturally accounted for in the framework of geometrical acoustics for  
30 instance by the approach of radiative energy transfer equations<sup>11-14</sup> and more recently by  
31 dynamical energy analysis<sup>15-17</sup>, these two approaches have the advantage to establish clearly

32 the link between geometrical acoustics and SEA<sup>18</sup> and even to propose a continuum between  
33 a full ray-tracing analysis and a more gross SEA analysis<sup>16</sup>.

34 In the wave approach of SEA<sup>19,20</sup>, the coupling power proportionality is naturally derived  
35 from the analysis in terms of plane waves impinging on the boundary separating the two  
36 subsystems<sup>21,22</sup>. The advantage of this approach is that it provides explicit formulas for the  
37 coupling loss factors that are also applicable to the case of non isotropic incidence. But this  
38 type of analysis is restricted to the hypothesis of rays and its main innuendo the principle of  
39 locality. In case of point connected subsystems, the applicability of locality is questionable  
40 although the coupling power proportionality remains valid.

41 There is however an interest to test the validity of the coupling power proportionality  
42 beyond the assumption of diffuse field in the most general case. Some particular effects  
43 may frustrate a uniform and isotropic distribution of energy and therefore may constitute  
44 an obstacle to application of SEA. For instance, symmetries in geometry can lead to a non-  
45 homogeneity of the field. In a circular plate, one observe the presence of a caustic passing  
46 through the point of excitation where the energy density has a higher level<sup>23</sup>. Vibrational  
47 energy is also enhanced on points and lines outside source position for spatial symmetry  
48 reasons<sup>24</sup>. This phenomenon is caused by an effect of coherence in ray propagation. This  
49 energy enhancement has been observed for instance by deflectometry<sup>25</sup> and with vibrational  
50 field measurements with a laser vibrometer<sup>26</sup>.

51 In this context, the objective of this study is to check if the coupling power proportion-  
52 ality is still valid for point connected subsystems in situations where the field is not fully  
53 homogeneous.

54 The paper is organized as follows. Section II reminds of theoretical aspects of SEA and  
55 proposes a local formulation of the coupling power proportionality. Section III presents four  
56 examples of vibrational fields for which the energy is not perfectly uniformly distributed.  
57 The validity of the local form of the coupling power proportionality is tested by numerical  
58 simulations in Section IV and by experiments in Section V. Finally, in Section VI, the notion  
59 of vibrational temperature is introduced and a thermodynamic interpretation of these results  
60 is proposed.

## 61 **II. BASICS OF SEA**

62 The principle of statistical energy analysis is to divide a complex system into simple  
63 subsystems and, for each subsystem, to estimate the power supplied by external sources, the  
64 losses of vibrational energy by natural processes of dissipation, and the exchange of energy  
65 with other subsystems.

### 66 **A. SEA assumptions**

67 The theory of statistical energy analysis requires three assumptions.

- 68 • (H1) The sources are random, stationary, wide band, and uncorrelated;
- 69 • (H2) The couplings between subsystems are conservative and weak;
- 70 • (H3) The vibrational field is diffuse in all subsystems.

71 These assumptions have been discussed in the literature (see Ref.<sup>27</sup> for a review of them)  
72 and some of them have been partly relaxed. The consequence of strong coupling is discussed

73 in Ref.<sup>28,29</sup>. The necessity of conservative coupling is justified in Ref.<sup>30</sup>. Since the purpose  
74 of this article is only to investigate the influence of diffuse field in the subsystems on SEA  
75 results, the rest of the discussion will be held under the condition that (H1) and (H2) apply.

76 The diffuse field assumption is certainly the most difficult to satisfy in practice. A diffuse  
77 field is defined as a homogeneous and isotropic superposition of plane waves whose phase is  
78 random.

79 A solution to obtain a diffuse field is to excite the structure with a uniform distribution  
80 of point forces which are  $\delta$ -correlated in space and time (rain-on-the-roof). In that case, all  
81 modes receive an equal amount of energy and if their damping ratio is the same, they store  
82 a same amount of energy.

83 With a single point force, the state of diffuse field is reached when the source is random  
84 and the structure sufficiently reverberant. Then, a large number of modes weakly damped  
85 contribute to the vibrational energy within the system. The number of resonant modes  
86 must be large to avoid a modal effect by a dominating mode and the damping must be low  
87 to ensure the mixing of energy by rays that propagate over a long range and are reflected  
88 throughout the subsystem.

89 To check if the vibrational field is diffuse in the subsystems validity diagrams have been  
90 proposed<sup>31</sup>. This diagram plots a criterion of uniformity of energy in the frequency, damping  
91 loss factor plane. The zone of diffuse field is confined by two lines marking the conditions  
92 of large number of resonant modes and weak attenuation of rays during a mean-free-path.  
93 Based on the location of each subsystem in these diagrams, it is possible to anticipate the  
94 applicability of SEA<sup>32</sup>.

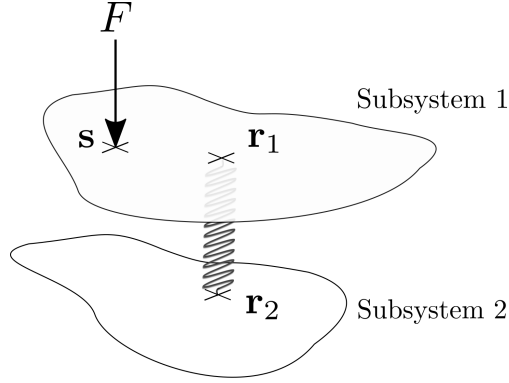


FIG. 1. Two flat subsystems coupled with a spring at point  $\mathbf{r}_1$  on plate 1 and point  $\mathbf{r}_2$  on plate 2.

Plate 1 is excited with a wide-band stationary random force  $F$  at point  $\mathbf{s}$ .

95 **B. The law of coupling power proportionality**

96 Let us consider two flat plates in flexural vibration weakly coupled by a spring attached  
 97 at point  $\mathbf{r}_1$  on plate 1 and point  $\mathbf{r}_2$  on plate 2 as shown in Figure 1. Subsystem 1 is excited  
 98 by a wide band random force  $F(t)$  at point  $\mathbf{s}$ . We assume that the field is diffuse in both  
 99 plates.

100 Under these conditions, the coupling power proportionality states that the expectation  
 101 of the power  $P$  (W) exchanged between connected subsystems is

$$P = \beta \left( \frac{E_1}{n_1} - \frac{E_2}{n_2} \right). \quad (1)$$

102 where  $E_i$  is the expectation of vibrational energy (J) in subsystem  $i$ ,  $n_i$  the modal density  
 103 (modes per rad/s), and  $\beta$  a dimensionless coefficient. In particular, this law shows that the  
 104 vibrational energy always flows from subsystems having a large modal energy to that with  
 105 a lower modal energy.

106 In the case of flat plates in flexural vibration, the modal density is given by

$$n_i = \frac{A_i}{4\pi} \sqrt{\frac{m_i}{D_i}} \quad (2)$$

107 where  $A_i$  is the area ( $\text{m}^2$ ),  $m_i$  is the mass per unit area ( $\text{kg}/\text{m}^2$ ), and  $D_i = E_i h_i^3 / 12(1 - \nu_i^2)$   
 108 the bending stiffness ( $\text{N}\cdot\text{m}$ ) with  $E_i$  the Young modulus ( $\text{Pa}$ ),  $h_i$  the thickness ( $\text{m}$ ) and  $\nu_i$   
 109 the Poisson coefficient of plate  $i$ . Note that the modal density of a plate does not depend  
 110 on the frequency and is proportional to its area.

111 When the plates are coupled by a spring of stiffness  $K$ , the coupling coefficient is

$$\beta = \frac{K^2}{32\pi\omega_c^2 \sqrt{m_1 m_2 D_1 D_2}} \quad (3)$$

112 where  $\omega_c$  is the central frequency ( $\text{rad}/\text{s}$ ) of the wide-band random source.

### 113 C. Generalized coupling power proportionality

114 Introducing the mean energy density  $e_i$  ( $\text{J}/\text{m}^2$ ) defined as  $e_i = E_i/A_i$  the energy per unit  
 115 area into Eq. (1) gives

$$P = \beta \left( \frac{e_1 A_1}{n_1} - \frac{e_2 A_2}{n_2} \right). \quad (4)$$

116 This form suggests a generalization to the case where the energy is not uniformly dis-  
 117 tributed into the subsystems. Substituting the local energy density  $e_i(\mathbf{r})$  at the coupling  
 118 point  $\mathbf{r}$  to the mean energy density  $e_i$  in Eq. (4) leads to

$$P = \beta \left( \frac{e_1(\mathbf{r}_1) A_1}{n_1} - \frac{e_2(\mathbf{r}_2) A_2}{n_2} \right). \quad (5)$$

119 where  $e_1(\mathbf{r}_1)$  and  $e_2(\mathbf{r}_2)$  are respectively the energy densities at point  $\mathbf{r}_1$  on subsystem 1 and  
 120 point  $\mathbf{r}_2$  on subsystem 2.

121 In Eq. (1) appear the modal energies  $E_i/n_i$ . Since most of modes expand over the whole  
 122 subsystem, these are global quantities. But Eq. (5) is written in terms of energy densities  
 123  $e_i(\mathbf{r})$  which are local quantities. Furthermore, the ratio  $A_i/n_i = 4\pi\sqrt{D_i/m_i}$  is also a local  
 124 since it only depends on local characteristics of the plate ( $m_i$  and  $D_i$ ).

125 When the vibratory fields are diffuse, Eqs. (1) and (5) are equivalent. However, it is  
 126 relevant to wonder if the latter remains valid in cases where the local energy density  $e_i(\mathbf{r})$   
 127 is not equal to the mean energy density  $e_i$ . The rest of the paper focuses on this question.

### 128 III. DIFFUSE AND NON-DIFFUSE FIELD

129 Three geometries of plates are considered: a Bunimovich stadium plate, a rectangular  
 130 plate, and a circular plate (see Fig. 2). These shapes have been chosen because they are  
 131 representative of various behaviours in ray propagation<sup>33</sup>. A Bunimovich stadium is a chaotic  
 132 billiard<sup>34</sup>. Almost all rays propagating and specularly reflecting on boundaries explore the  
 133 entire phase space (all positions and all directions) with an equal probability of presence.  
 134 The vibrational field resulting from a large number of rays emitted by a single source is  
 135 therefore naturally diffuse.

136 A rectangular billiard is an integrable dynamical system. A ray does not generally explore  
 137 the entire phase space. It generally passes near all points of the rectangle excepted if its  
 138 path is closed. But the angle of incidence is always the same on small edges and the same  
 139 (with possibly a different value) on large edges (with positive or negative sign). Thus the  
 140 ray can take only four directions during its propagation. The resulting field is therefore

141 homogeneous but not isotropic. However, if a point source emits many rays equally in all  
 142 directions, then it enforces the field to be isotropic and therefore to be diffuse.

143 A circular billiard is also an integrable dynamical system. The angle of incidence of a  
 144 ray on the boundary is constant during its propagation. The ray forms a circular caustic  
 145 that never get into. Thus the ray explores entirely the part of the disk located outside this  
 146 circular caustic excepted if its path is closed. But the ray does not explore the part of the  
 147 disk located inside the circular caustic. The phase space is not entirely explored and the  
 148 resulting vibrational field is never diffuse neither with a single ray nor with an isotropic  
 149 source emitting rays in all directions.

#### 150 **A. Direct numerical simulation of energy field**

151 In all subsequent numerical simulations, the values of the mechanical parameters are the  
 152 followings. The Young modulus is  $E = 203$  GPa, the mass density  $\rho = 8010$  kg.m<sup>-3</sup> and  
 153 Poisson's ratio  $\nu = 0.3$ . The thickness of the three plates is  $h = 2$  mm. Their dimensions  
 154 are represented in Figure 2. They all have an area about  $A = 0.25$  m<sup>2</sup>. Two values of  
 155 the damping loss factor are used:  $\eta = 0.002$  in case of light damping and  $\eta = 0.2$  when  
 156 the damping is strong. A unique external force  $F(t)$  is applied to plate 1 at point  $\mathbf{s}$ . The  
 157 excitation point is located at  $x=176$  mm,  $y=164$  mm in the stadium plate, at  $x=120$  mm,  
 158  $y=70$  mm in the rectangular plate, and at  $x=150$  mm,  $y=150$  mm in the circular plate. The  
 159 force is a stationary random process of power spectral density  $S_0$  constant in the octave  
 160 band  $\Delta\omega$  centred on  $\omega_c = 2\pi \times 4000$  rad.s<sup>-1</sup> and zero elsewhere.

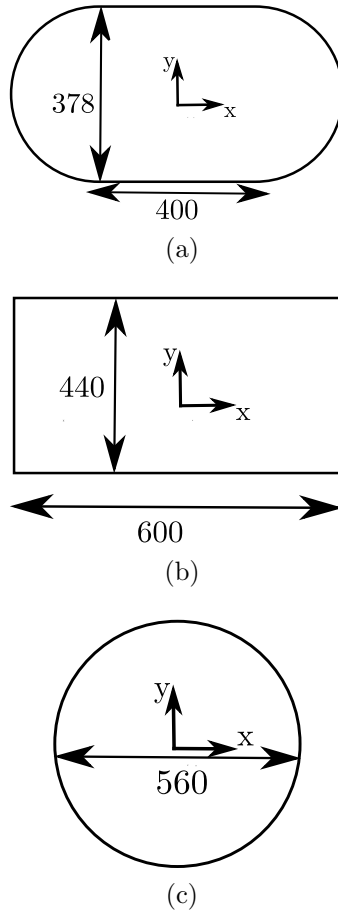


FIG. 2. Shape and dimensions of plates in mm. (a); Bunimovich stadium, (b); Rectangular plate, and (c); Circular plate.

161 With these values, we may estimate the mean-free-path  $\bar{l} = \pi A/P$  where  $A$  is the plate  
 162 area and  $P$  the perimeter. For the stadium plate  $\bar{l} = 0.42$  m, for the rectangular plate  
 163  $\bar{l} = 0.40$  m, and for the circular plate  $\bar{l} = 0.44$  m. The group velocity is  $c_g = 553$  m/s and  
 164 the wavelength is  $\lambda = 7$  cm at 4 kHz which is six times lower than the mean-free-path. This  
 165 justifies that a geometrical acoustics approximation applies. The modal density is about  
 166 0.0065 mode per rad/s and therefore the number of resonant modes in the octave band  
 167 4 kHz is about  $N = 120$  which is high enough to consider a statistical population of modes.

168 Finally, the attenuation per mean-free-path is  $\bar{m} = \eta\omega\bar{l}/c_g$  is  $\bar{m} = 0.04$  when the damping  
 169 is light ( $\eta = 0.002$ ). This means that  $1 - \exp(-\bar{m}) = 4\%$  of the energy is lost between two  
 170 successive reflections of a ray. This low value ensures that rays experience a large number  
 171 of reflections before to vanish. But this value grows up to 98 % when the damping is high  
 172 ( $\eta = 0.2$ ) meaning that rays loss almost all their energy before the first reflection.

173 The expectation of vibrational energy density  $e(\mathbf{r})$  at position  $\mathbf{r}$  is  $e(\mathbf{r}) = m \langle \dot{u}^2 \rangle$   
 174 where  $\dot{u}$  is the vibrational velocity and  $\langle . \rangle$  denotes the random expectation operator.  
 175 The variance of  $\dot{u}$  is  $\int S_{\dot{u}\dot{u}} d\omega/2\pi$  where  $S_{\dot{u}\dot{u}}$  is the power spectral density of  $\dot{u}$ . In addition,  
 176  $S_{\dot{u}\dot{u}} = S_0\omega^2|H|^2$  where  $H(\mathbf{r}, \mathbf{s}; \omega)$  is the receptance (frequency response function between the  
 177 force  $F$  at point  $\mathbf{s}$  and deflection  $u$  at point  $\mathbf{r}$ ). Since the power spectral density  $S_0$  of the  
 178 force is constant within  $\Delta\omega$ , this gives

$$e(\mathbf{r}) = \frac{mS_0}{\pi} \int_{\Delta\omega} \omega^2 |H(\mathbf{r}; \mathbf{s}; \omega)|^2 d\omega. \quad (6)$$

179 In the numerical estimation of this integral, the angular frequency step is chosen as  $\omega\eta/4\sqrt{2}$ .  
 180 The receptance  $H(\mathbf{r}, \mathbf{s}; \omega)$  in terms of natural frequencies  $\omega_n$  and mode shapes  $\Psi_n$  is obtained  
 181 with a modal expansion

$$H(\mathbf{r}; \mathbf{s}; \omega) = \sum_{n>0} \frac{\Psi_n(\mathbf{s})\Psi_n(\mathbf{r})}{m(\omega_n^2 - \omega^2 + i\eta\omega_n\omega)}. \quad (7)$$

182 where  $i$  is the imaginary unit. The modes are calculated by the finite element method with  
 183 MSC/NASTRAN 2021.1 up to the frequency 6 kHz to ensure that  $H(\mathbf{r}; \mathbf{s}; \omega)$  is correctly  
 184 estimated within the entire octave band 4 kHz. About 240 modes have been found.

185 The inverse participation ratio is defined as the fourth-order moment of vibrational ve-  
 186 locity  $\dot{u}$  or equivalently as the second-order moment of energy density  $e(\mathbf{r})$

$$I_p = \frac{\frac{1}{A} \int e^2(\mathbf{r}) \, d\mathbf{r}}{\left(\frac{1}{A} \int e(\mathbf{r}) \, d\mathbf{r}\right)^2}. \quad (8)$$

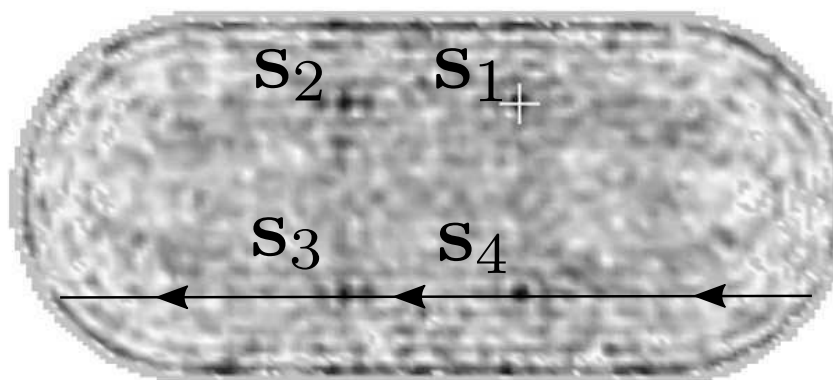
187 Its definition imposes  $I_p \geq 1$ . When the vibrational energy is uniformly distributed over  
 188 the subsystem ( $e(\mathbf{r}) = \text{cste}$ ),  $I_p$  goes to one. But when the vibrational energy distribution  
 189 is not uniform and presents large fluctuations from one point to another one,  $I_p$  can take  
 190 arbitrarily high values. We shall adopt the criterion  $I_p \leq 2$  to characterize a uniform  
 191 distribution of energy.

## 192 B. Diffuse field

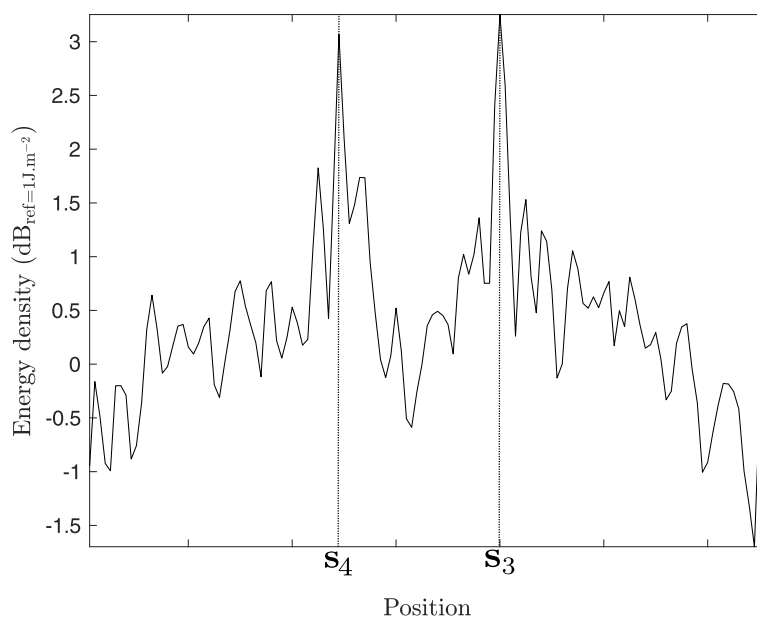
193 Fig. 3(a) shows the distribution of energy density in a lightly damped stadium-shaped  
 194 plate with clamped edges excited by a random force at point  $S_1$ . Fig. 3(b) shows the  
 195 distribution of energy density in a lightly damped rectangular plate with simply supported  
 196 edges excited by a random force.

197 The values of  $I_p$  for stadium and rectangular plates are given in Table I. They are both  
 198 lower than 2 (respectively 1.09 for the stadium and 1.38 for the rectangle) so that following  
 199 this criterion, the vibrational field is uniformly distributed over the rectangular plate and  
 200 the stadium.

201 But even if the inverse participation ratio is low, the vibrational field is not fully spatially  
 202 homogeneous. The energy distribution exhibits patterns with energy enhancement. For the  
 203 stadium shape, four points with energy enhancement are visible. They are noted  $\mathbf{s}_1, \mathbf{s}_2, \mathbf{s}_3,$

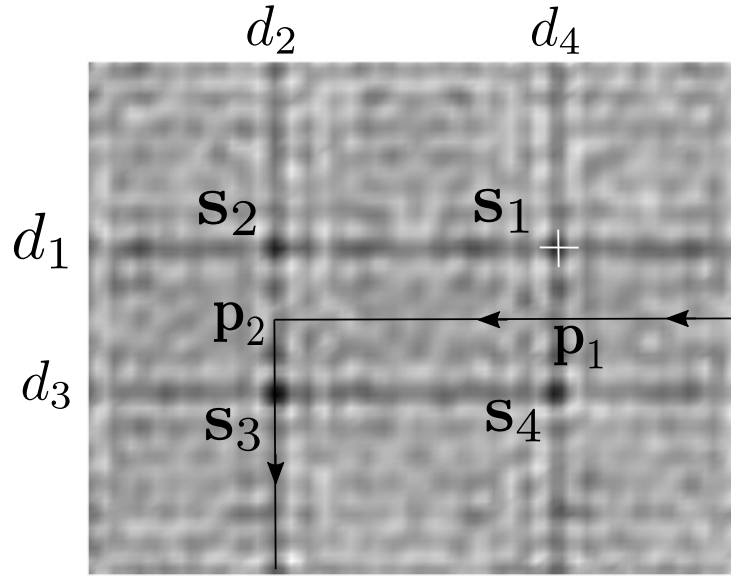


(a)

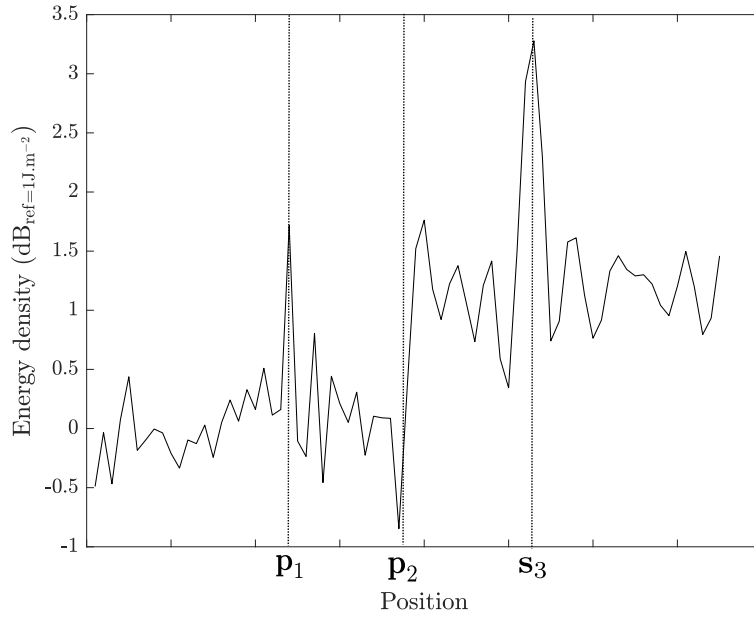


(b)

FIG. 3. (a) Numerical simulation of vibrational energy distribution (dB) in a stadium thin plate lightly damped ( $\eta = 2 \times 10^{-3}$ ) with clamped edges and excited by a wide-band random force. The cross indicates the force position. (b) Vibrational energy in dB along the black line.



(a)



(b)

FIG. 4. (a) Numerical simulation of vibrational energy distribution (dB) in a rectangular thin plate lightly damped ( $\eta = 2 \times 10^{-3}$ ) with simply supported edges and excited by a wide-band random force. The cross indicates the force position. (b) Vibrational energy in dB along the black line.

TABLE I. Inverse participation ratio for the four plates excited by a random force in the octave centred on 4 kHz.

	Stadium $\eta = 2 \times 10^{-3}$	Rectangle $\eta = 2 \times 10^{-3}$	Circle $\eta = 2 \times 10^{-3}$	Rectangle $\eta = 0.2$
IPR	1.09	1.38	8.89	4.61

204 and  $\mathbf{s}_4$  in Fig. 3(a). The enhancement factor on these four points is equal to 2 (this effect  
 205 at the source point is known as coherent backscattering effect<sup>34</sup>). In Fig. 3(b), we can see  
 206 lines noted  $d_1$ ,  $d_2$ ,  $d_3$ , and  $d_4$  which form a tic-tac-toe pattern with the driving point at one  
 207 of the four intersections. In Fig. 4(a), we see a step of about 1.5 dB on points  $\mathbf{p}_1$  and  $\mathbf{p}_2$ .  
 208 In linear scale, the enhancement factor of energy on these four lines is equal to  $3/2$ . On  
 209 the four points noted  $\mathbf{s}_1$ ,  $\mathbf{s}_2$ ,  $\mathbf{s}_3$ , and  $\mathbf{s}_4$  located at the intersections of the four lines, the  
 210 enhancement factor is equal to  $9/4$  (3.4 dB on point  $\mathbf{s}_3$  in Fig. 4(a)).

211 Several works have shown that a symmetrical mechanical structure excited by a wideband  
 212 random point force exhibits a pattern of points or lines where the vibrational response is  
 213 enhanced (see for instance Ref.<sup>26</sup> where a proof of these enhancement factor based on the  
 214 image source method is provided). These enhancements may be explained in geometrical  
 215 acoustics by considering the phase of pairs or quadruplets of rays arriving at the receiver  
 216 points with same phase. They interfere constructively and therefore contribute to the local  
 217 energy density more than the simple sum of their energies.

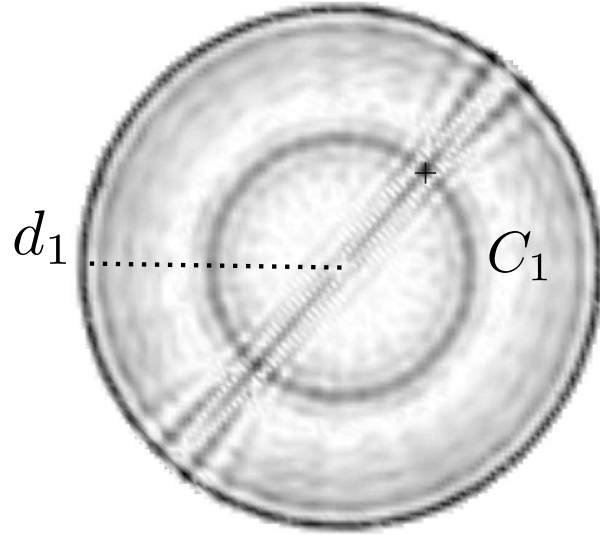
218 **C. Non diffuse field**

219 Fig. 5(a) shows the distribution of energy density in a lightly damped circular plate  
 220 with clamped edges excited by a random force at point  $S_1$ . The damping loss factor is low  
 221  $\eta = 2 \times 10^{-3}$ .

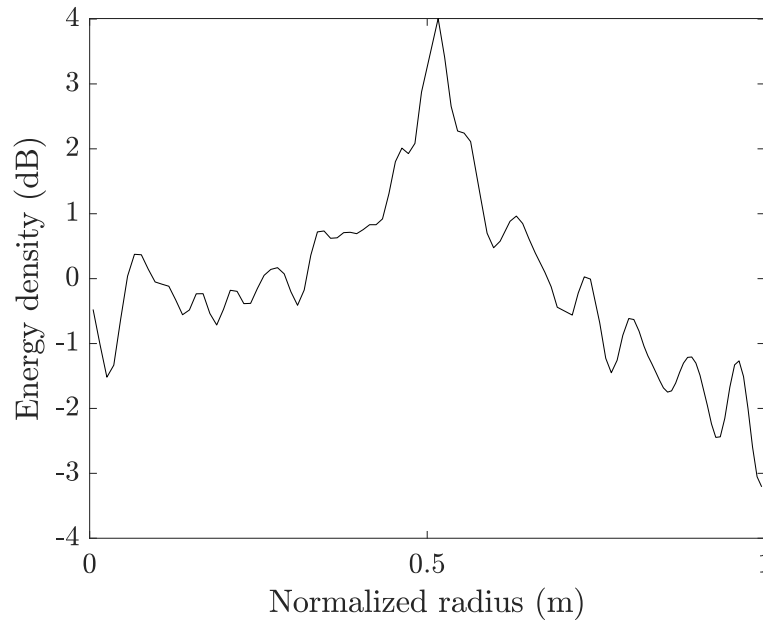
222 From Fig. 5(a) we see that the vibrational energy fluctuates a lot and reaches a maximum  
 223 on the circle  $C_1$  passing through the excitation point. Furthermore, the diameter passing  
 224 through the source also shows a higher level of energy. The inverse participation ratio is  
 225 high (8.89).

226 The evolution of energy density along a diameter can be explained again with ge-  
 227 ometrical acoustics. Each ray starting from the source turns into the circle by conserving  
 228 its angle of reflection. Excepted for periodic orbits, the ray forms a circular caustic that is  
 229 never crossed by it. The ray does not explore the entire disk and the resulting distribution  
 230 of energy is henceforth not uniform. The combination of large number rays emitted in all  
 231 directions from the source point gives roughly the distribution of energy observed in Fig.  
 232 5(b). It is not necessary to invoke interference of rays to explain this distribution.

233 The enhancement of energy on the diameter passing through the source point stems from  
 234 another phenomenon. This is again a phenomenon of constructive interference. The spatial  
 235 symmetry of the circle imposes that each ray starting from the source and arriving at any  
 236 point of this diameter, admits a symmetrical ray starting from the source and arriving at  
 237 the same point. Both direct and symmetrical rays have same length and therefore have the  
 238 same phase at arrival. They interfere constructively giving the observed enhancement.



(a)



(b)

FIG. 5. (a) Numerical simulation of vibrational energy distribution (dB) in a circular thin plate lightly damped ( $\eta = 2 \times 10^{-3}$ ) with clamped edges and excited by a wide-band random force. The cross indicates the force position. (b) Vibrational energy in dB along the radius  $d_1$ .

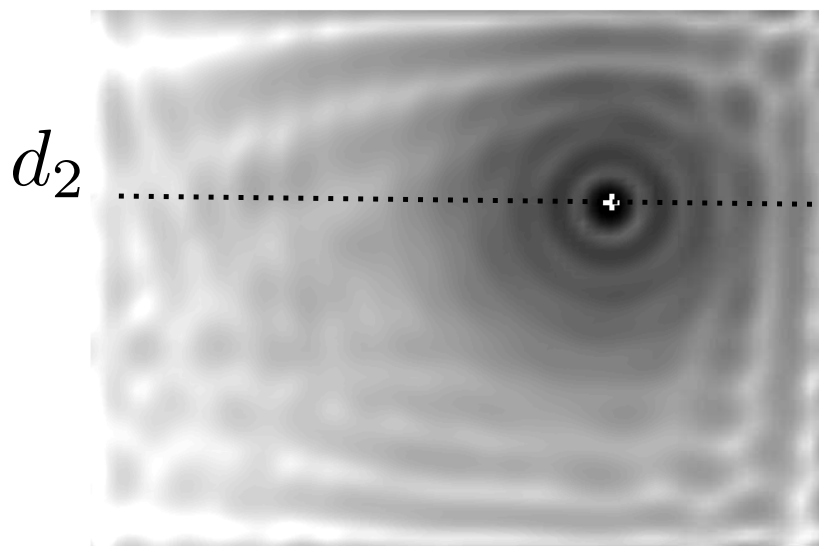
239 A last cause of breaking homogeneity is the influence of strong dissipation. Fig. 6(a)  
 240 shows the distribution of energy density in a highly damped ( $\eta = 0.2$ ) rectangular plate  
 241 with simply supported edges excited by a random force at point  $S_1$ . Fig. 6(a)a shows the  
 242 maps of energy density and Fig. 6(b) shows the vibrational energy along the line  $d_2$  while  
 243 the dashed line is obtained with a reference calculation.

244 We observe that the distribution of energy is clearly not uniform which is confirmed by  
 245 the high value (4.61) of the inverse participation. The maximum of energy is reached at the  
 246 source point from which the energy strongly decreases in a axi-symmetrical way.

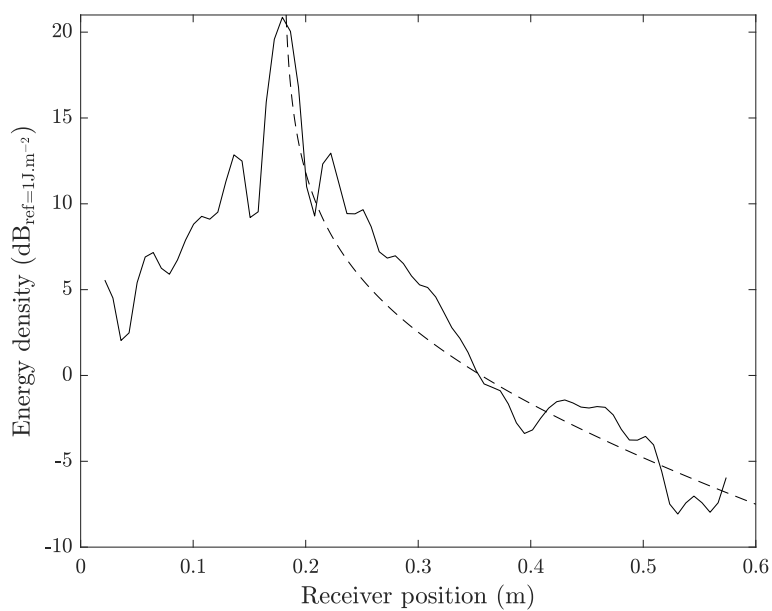
247 We know that the attenuation per mean-free-path is high ( $\bar{m} = 3.6$ ) and that rays loss  
 248 98 % of their energy before the first reflection. The vibrational field is therefore dominated  
 249 by the direct field and the reflected field remains negligible. For the direct field, the energy  
 250 at distance  $R$  from the source is  $\exp(-mR)/2\pi c_g R$ . The exponential term is the dissipation  
 251 while the second term is due to the geometric scattering. In Fig. 6(b), we observe that  
 252 the dashed line (direct field) and the solid line (actual field including reverberation) well fit  
 253 which confirms the domination of the direct field in the actual field.

#### 254 IV. NUMERICAL SIMULATION OF EXCHANGED POWER

255 Let us now turn to the verification of the generalized coupling power proportionality (5)  
 256 by a numerical approach.



(a)



(b)

FIG. 6. (a) Numerical simulation of vibrational energy distribution (dB) in a rectangular thin plate highly damped ( $\eta = 0.2$ ) with simply supported edges and excited by a wide-band random force. The cross indicates the force position. (b) Vibrational energy in dB along the radius  $d_2$ .

257 **A. Principle of the simulation**

258 We consider again the three geometries of plates introduced in Section III: the stadium,  
 259 the rectangle, and the disk. But now, the plates are mechanically coupled by a spring  
 260 of stiffness  $K$ . Each numerical test case consists in two similar plates among the three  
 261 geometries coupled by the spring whose position may vary to explore zones with different  
 262 levels of vibrational energy. The spring is attached at point  $\mathbf{r}_1$  on plate 1 and at  $\mathbf{r}_2$  centre of  
 263 plate 2. Plate 1 is excited at point  $\mathbf{s}$  always with a random force of power spectral density  $S_0$   
 264 constant in the octave band  $\Delta\omega$ . The positions of the point force are the same as in Section  
 265 III. The exact positions  $\mathbf{r}_1$  of the spring will be specified in each numerical simulation.

266 The expectation of vibrational energy density  $e_i(\mathbf{r})$  in plates 1 and 2 is calculated again by  
 267 Eq. (6). The only difference is concerned with the receptance  $H$  which is now the receptance  
 268 of the *coupled* system. Thus,  $H(\mathbf{r}, \mathbf{s}; \omega)$  denotes the deflection at point  $\mathbf{r}$  (in plate 1 or 2) of  
 269 the coupled system excited at point  $\mathbf{s}$  (in plate 1).

270 The expectation of exchanged power via the spring is  $P = K \langle (u_2 - u_1)\dot{u}_1 \rangle = K \langle$   
 271  $u_2\dot{u}_1 \rangle = -K \langle \dot{u}_2 u_1 \rangle$  where  $u_i$  is the deflection of plate  $i$  at the coupling point. In terms  
 272 of receptance, this power becomes

$$P = \frac{KS_0}{\pi} \int_{\Delta\omega} \text{Re}[i\omega \overline{H}(\mathbf{r}_1, \mathbf{s}; \omega)H(\mathbf{r}_2, \mathbf{s}; \omega)] d\omega \quad (9)$$

273 where  $\text{Re}$  denotes the real part, the overbar the complex conjugate, and  $i$  the imaginary  
 274 unit.

275 The numerical simulation is conducted with the same modes of isolated plates calculated  
 276 by MSC/NASTRAN in Section II. But instead of using Eq. (7) to calculate  $H$ , the receptance

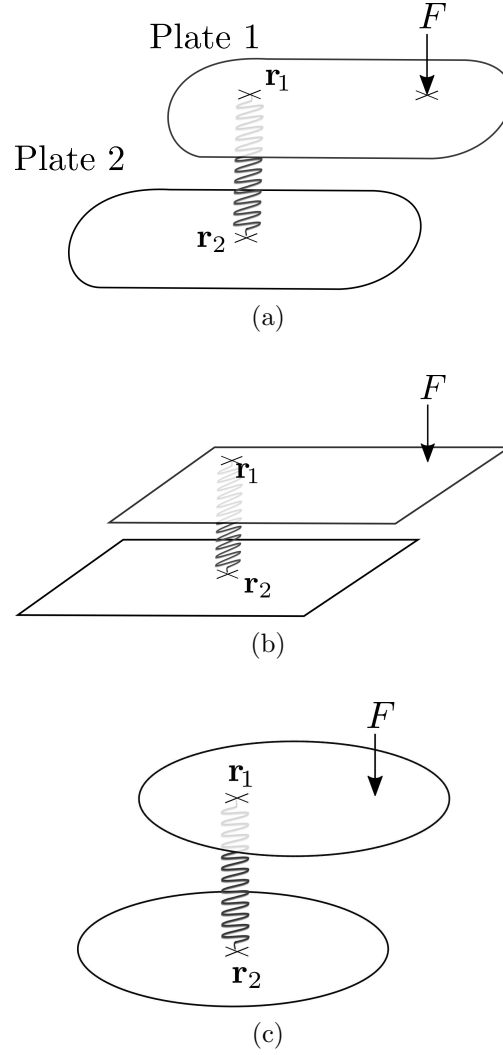


FIG. 7. (a) The stadium-shaped plates, (b) the rectangular plates, and (c) the disk plates coupled with a spring.

277 of coupled system is derived from the receptances of uncoupled subsystems by introducing  
 278 the deflections  $u_1, u_2$  at both ends of the spring as unknown and solving a set of two linear  
 279 equations to determine them (the exact procedure is detailed in Appendix A).

280 Once, we have computed the energies  $e_1(\mathbf{r}_1), e_2(\mathbf{r}_2)$  and the exchanged power  $P$  by the  
 281 above procedure, the coupling coefficient  $\beta$  is estimated by

$$\beta = \frac{P}{\frac{e_1(\mathbf{r}_1)A_1}{n_1} - \frac{e_2(\mathbf{r}_2)A_2}{n_2}}. \quad (10)$$

282 In particular, we shall compare the numerical determination of  $\beta$  by Eq. (10) with its  
 283 theoretical value given in Eq. (3).

## 284 B. Test cases

285 All numerical simulations of this Section are conducted on plates whose geometrical and  
 286 mechanical parameters are those of Section III. In particular, the frequency of excitation is  
 287  $\omega_c = 2\pi \times 4000$  rad/s and the wavelength is 7 cm to be compared with a mean-free-path  
 288 of 42 cm. The number of resonant modes is about 120 per subsystem that is 240 for the  
 289 whole system. The spring stiffness is  $K = 1.10^5$  N/m. To ensure that the weak coupling  
 290 assumption is satisfied, the coupling loss factor defined as  $\eta_{12} = \beta/\omega_c n_1$  has to be lower than  
 291 the damping loss factor  $\eta^{28}$ . The coupling loss factors  $\eta_{12} = \eta_{21}$  are equal to  $3.10^{-6}$  which is  
 292 lower than the damping loss factor ( $2.10^{-3}$ ) and so the coupling is weak enough.

293 Four simulations are carried out with the four types of diffuse and non-diffuse fields  
 294 presented in Section III.

### 295 1. Stadium plate

296 The numerical simulation with two coupled stadium plates is presented in Fig. 8(a).  
 297 In the inset of Fig. 8(a) the stadium is represented and the four points with an energy  
 298 enhancement of 2 are noted  $\mathbf{s}_1$  (the source),  $\mathbf{s}_2$ ,  $\mathbf{s}_3$ , and  $\mathbf{s}_4$ . Four other points noted 1

299 to 4 are chosen at random inside the zone where the field is diffuse. Fig. 8(a) shows a  
 300 comparison between the exchanged power  $P$  determined by Eq. (9) and the difference of  
 301 local energies  $e_1(\mathbf{r}_1)A_1/n_1 - e_2(\mathbf{r}_2)A_2/n_2$  where  $e_i$  is determined by Eq. (6). The bold line  
 302 with the crosses represents the power exchanged between the two plates. The thin line with  
 303 the stars represents the difference of the local energies. Fig. 8(b) presents the relative error  
 304 between  $\beta$  determined by Eq. (3) and by Eq. (10).

305 First, the spring is successively attached at the four points 1 to 4 where the vibrational  
 306 field is diffuse. It can be seen in Fig. 8(b) that the ratio of  $P$  and  $e_1(\mathbf{r}_1)A_1/n_1 - e_2(\mathbf{r}_2)A_2/n_2$   
 307 (or difference in log-scale) is almost the same for the four points. Furthermore we see in Fig.  
 308 8(b) that this ratio is close to the theoretical value of  $\beta$  given in Eq. (3).

309 Secondly, the spring is successively attached at the four points  $\mathbf{s}_1$ ,  $\mathbf{s}_2$ ,  $\mathbf{s}_3$ , and  $\mathbf{s}_4$ . The  
 310 exchanged power is increased by a step of  $10 \log(2)$  which corresponds exactly to the en-  
 311 hancement factor of 2. Again, the ratio of  $P$  and  $e_1(\mathbf{r}_1)A_1/n_1 - e_2(\mathbf{r}_2)A_2/n_2$  is close to the  
 312 theoretical  $\beta$ .

313 In all cases, the numerical coupling coefficient is found to be in fine agreement with the  
 314 theoretical value. The mean relative error between the numerical and theoretical values is  
 315 28.8 %.

## 316 **2. Rectangular plate with light damping**

317 The numerical simulation with two coupled rectangular plates is presented in Fig. 9(a).  
 318 In the inset of Fig. 9(a) the rectangular plate is represented with the four lines presenting  
 319 an energy enhancement of  $3/2$ . The five points ( $\mathbf{d}_1$ ,  $\mathbf{d}_2$ ,  $\mathbf{d}_3$ ,  $\mathbf{d}_4$  and  $\mathbf{d}_5$ ) are chosen randomly

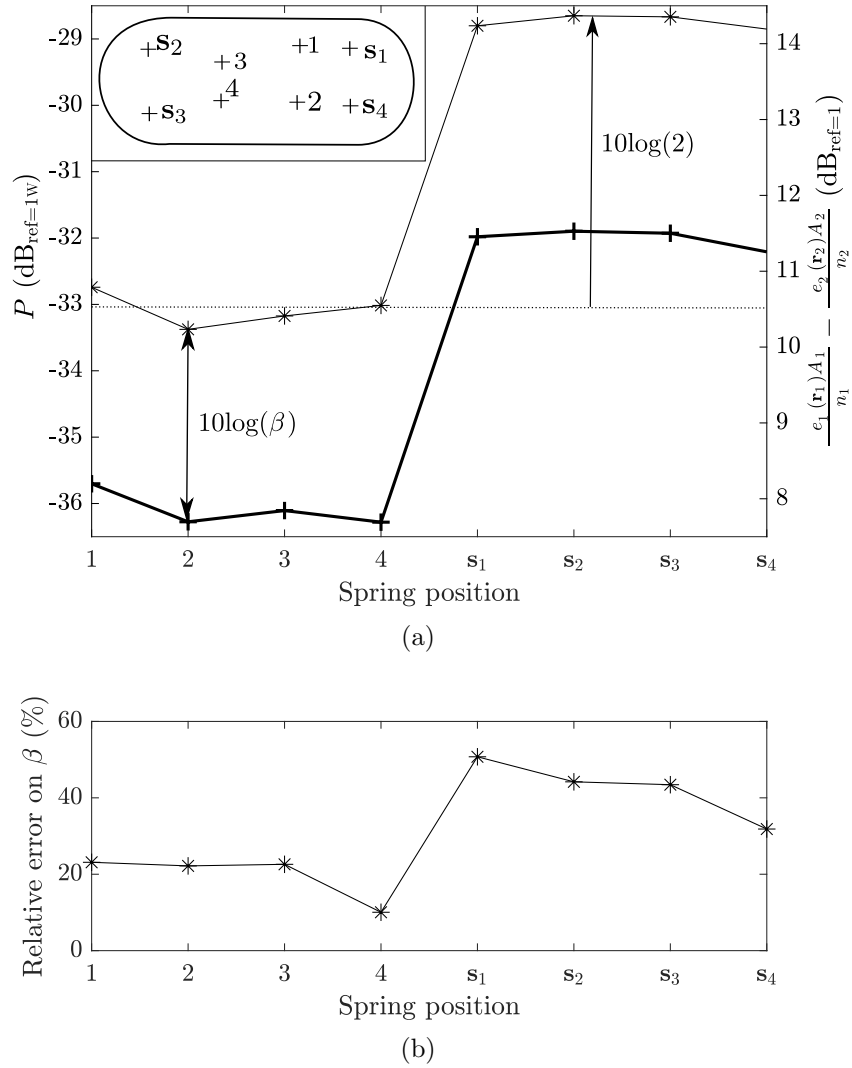


FIG. 8. (a) Comparison between the exchanged power and the difference of local energies. The bold line with the crosses represents the power exchanged between the two plates. The thin line with the stars represents the difference of the local energies. In the insert: stadium plates excited with a random white noise at point  $s_1$ . Points with an energy enhancement equal to 2 are noted  $s_1$ ,  $s_2$ ,  $s_3$ , and  $s_4$ . The spring is successively attached to the points noted  $s_1$ ,  $s_2$ ,  $s_3$ ,  $s_4$ , 1, 2, 3 and 4. (b) Relative error between the coupling coefficient predicted theoretically with Eq. (3) and numerically with Eq. (10) for two coupled stadium plates excited by a point force on plate 1.

320 on these four lines. The four points of energy enhancement  $9/4$  ( $\mathbf{s}_1$ ,  $\mathbf{s}_2$ ,  $\mathbf{s}_3$ , and  $\mathbf{s}_4$ ) are  
 321 represented with a cross. Five points noted 1 to 5 are chosen at random inside the zone  
 322 where the field is diffuse. Fig. 9(a) shows a comparison between the exchanged power  $P$   
 323 determined by Eq. (9) and the difference of local energies  $e_1(\mathbf{r}_1)A_1/n_1 - e_2(\mathbf{r}_2)A_2/n_2$  where  
 324  $e_i$  is determined by Eq. (6). Fig. 9(b) presents the relative error between  $\beta$  determined by  
 325 Eq. (3) and by Eq. (10).

326 First, the spring is successively attached at the five points 1 to 5 where the vibrational  
 327 field is diffuse. It can be seen in Fig. 9(a) that the ratio of  $P$  and  $e_1(\mathbf{r}_1)A_1/n_1 - e_2(\mathbf{r}_2)A_2/n_2$   
 328 is almost the same for the five points. Furthermore we see in Fig. 9(b) that this ratio is  
 329 close to the theoretical value of  $\beta$  given in Eq. (3).

330 Secondly, the spring is successively attached on a point located on a line ( $\mathbf{d}_1$ ,  $\mathbf{d}_2$ ,  $\mathbf{d}_3$ , and  
 331  $\mathbf{d}_4$ ). The exchanged power is increased by a step of  $10 \log(3/2)$  which corresponds to the  
 332 enhancement factor of  $3/2$ . Once again, the ratio of  $P$  and  $e_1(\mathbf{r}_1)A_1/n_1 - e_2(\mathbf{r}_2)A_2/n_2$  is  
 333 almost the same for the four points and this ratio is close to the theoretical value of  $\beta$ .

334 Thirdly, the spring is successively attached on a point located at the intersection of the  
 335 lines ( $\mathbf{s}_1$ ,  $\mathbf{s}_2$ ,  $\mathbf{s}_3$ , and  $\mathbf{s}_4$ ). The exchanged power is increased by a step of  $10 \log(9/4)$  which  
 336 corresponds to the enhancement factor of  $9/4$ . The ratio of the exchanged power  $P$  and  
 337  $e_1(\mathbf{r}_1)A_1/n_1 - e_2(\mathbf{r}_2)A_2/n_2$  is almost the same for the four points and this ratio is close to  
 338 the theoretical value of  $\beta$ .

339 Whatever the position of the spring attachment, the value of  $\beta$  is found to be in fine  
 340 agreement with the theoretical value. The mean error is 31.02%.

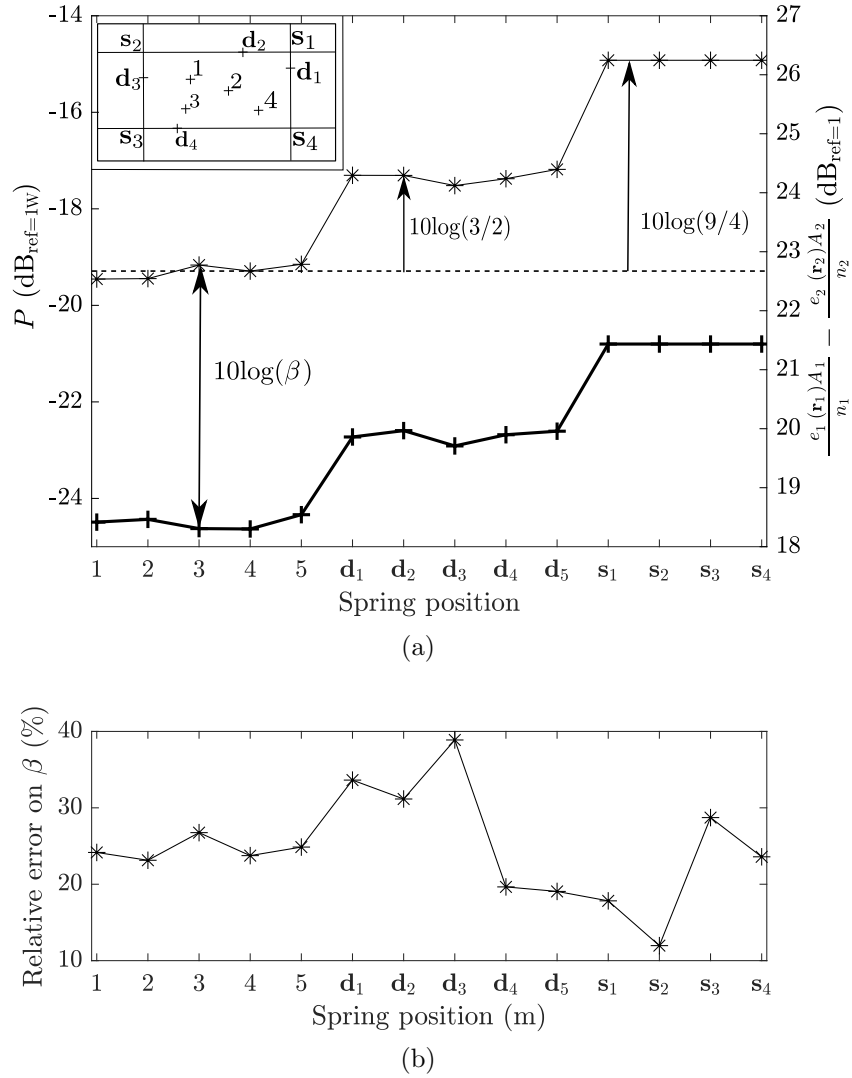


FIG. 9. (a) Comparison between the exchanged power and the difference of local energies. The bold line with the crosses represents the power exchanged between the two plates. The thin line with the stars represents the difference of the local energies. In the insert: Rectangular plate excited with a random white noise at point  $s_1$ . Lines with an energy enhancement equal to  $3/2$  are represented with lines and the energy enhancement at these lines intersections is  $9/4$ . The spring is successively attached to the points noted  $s_1, s_2, s_3, s_4, d_1, d_2, d_3, d_4, d_5, 1, 2, 3, 4$  and  $5$ . (b) Relative error between the coupling coefficient predicted theoretically with Eq. (3) and numerically with Eq. (10) for two coupled rectangular plates excited by a point force on plate 1.

341 **3. Circular plate**

342 The numerical simulation with two coupled circular plates is presented in Fig. 10(a).  
 343 The circular plate is shown in the inset Fig. 10(a). The source is located at point  $\mathbf{s}_1$ .  
 344 The energy enhancement is represented with the dashed circle noted  $C_1$ . Fig. 10(a) shows a  
 345 comparison between the exchanged power  $P$  and the difference of local energies  $e_1(\mathbf{r}_1)A_1/n_1 -$   
 346  $e_2(\mathbf{r}_2)A_2/n_2$ . Fig. 10(b) shows the relative error between  $\beta$  determined by Eq. (3) and by  
 347 Eq. (10).

348 The exchanged power  $P$  and the difference of local energies  $e_1(\mathbf{r}_1)A_1/n_1 - e_2(\mathbf{r}_2)A_2/n_2$   
 349 are calculated for 108 points along the radius  $d_1$ . It can be seen in Fig. 10(a) that the energy  
 350 is higher on the circle passing through the excitation point and decreases inside and outside  
 351 of this circle. The ratio of the exchanged power  $P$  and the difference of the local energies  
 352  $e_1(\mathbf{r}_1)A_1/n_1 - e_2(\mathbf{r}_2)A_2/n_2$  is almost the same for all the points and this ratio is very similar  
 353 to the theoretical value of  $\beta$ .

354 The coupling coefficient is found to be in fine agreement with the theoretical value. The  
 355 mean relative error between the numerical and theoretical value of  $\beta$  is 36.8%.

356 **4. Rectangular plate with high damping**

357 The numerical simulation with two rectangular plates with high damping is presented  
 358 in Fig. 11(a). The rectangular plate is shown in the inset of Fig. 11(a). Fig. 11(a)  
 359 shows a comparison between the exchanged power  $P$  and the difference of local energies

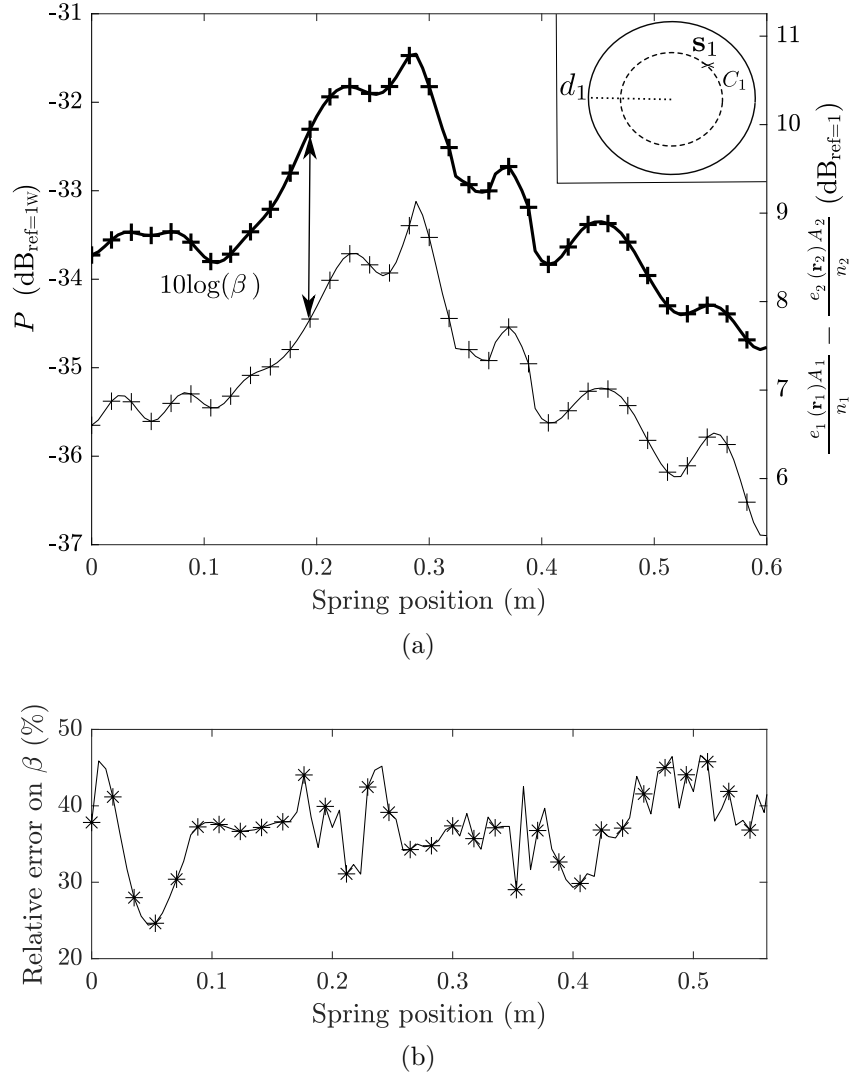


FIG. 10. (a) Comparison between the exchanged power and the difference of local energies. The bold line with the crosses represents the power exchanged between the two plates. The thin line with the stars represents the difference of the local energies. In the insert: Circular plate excited with a random white noise at point  $s_1$  on the plate 1. The circle with an energy enhancement is noted  $C_1$ . The spring is successively attached to 108 points along the line  $d_1$ . (b) Relative error between the coupling coefficient predicted theoretically with Eq. (3) and numerically with Eq. (10).

360  $e_1(\mathbf{r}_1)A_1/n_1 - e_2(\mathbf{r}_2)A_2/n_2$ . Fig. 11(b) presents the relative error between  $\beta$  determined by  
 361 Eqs. (3) and (10).

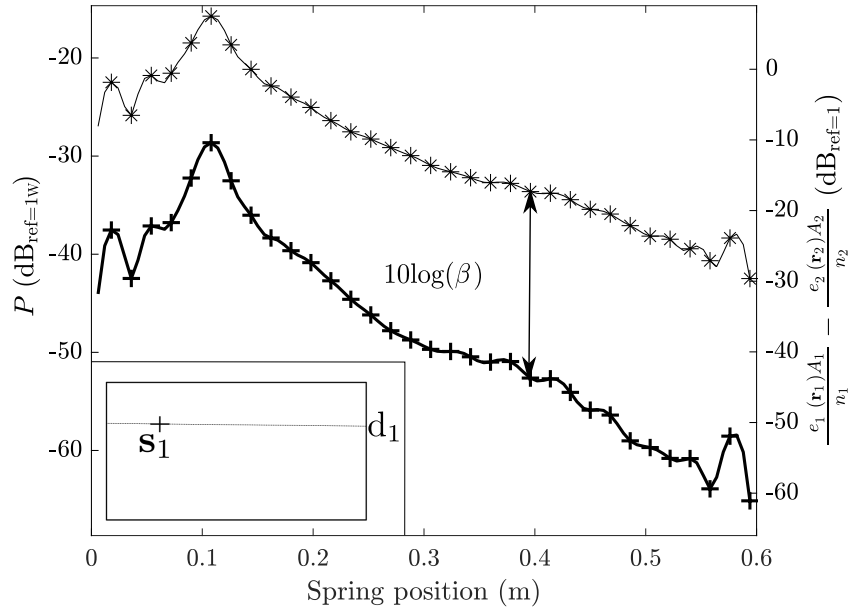
362 The spring is successively attached at the 108 points along the line  $d_1$ . We see in Fig.  
 363 11(a) that the exchanged power evolves proportionally to the difference of the local energies.  
 364 The difference of local energies and the exchanged power are very high at the vicinity of the  
 365 source point and decrease rapidly. The ratio of  $P$  and  $e_1(\mathbf{r}_1)A_1/n_1 - e_2(\mathbf{r}_2)A_2/n_2$  is almost  
 366 the same for the 108 points. Furthermore we see in Fig. 11(b) that this ratio is close to the  
 367 theoretical value of  $\beta$  given in Eq. (3). The mean relative error between the numerical and  
 368 the theoretical value of  $\beta$  is 14.06%. This proves that the coupling coefficient is still valid  
 369 with non diffuse field caused by high damping.

## 370 V. MEASUREMENT OF EXCHANGED POWER

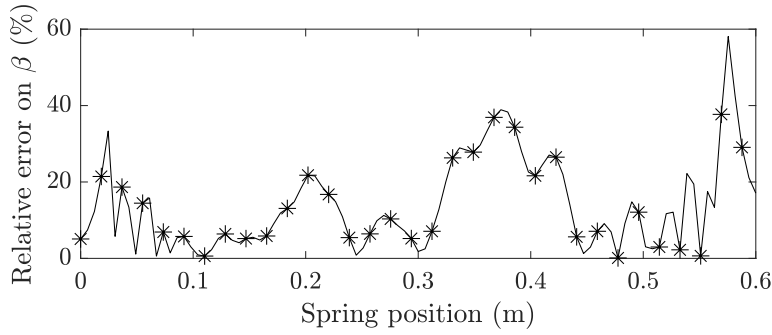
371 Finally, we present measurements of the power exchanged between two rectangular plates  
 372 coupled with a spring to verify the generalized coupling power proportionality (Eq. 5).

### 373 A. Principle of the experiment

374 The experimental set-up is shown in Fig. 12. The plates are suspended from a rigid  
 375 frame with bungee cords attached to the plates by small holes. The two plates are coupled  
 376 with a spring of stiffness  $K=431 \text{ N.m}^{-1}$  held by magnets. The plates are made of stainless  
 377 steel. The mechanical characteristics of the plates are exactly the same as in Section III  
 378 excepted that the boundary conditions are now free.



(a)



(b)

FIG. 11. (a) Comparison between the exchanged power and the difference of local energies. The bold line with the crosses represents the power exchanged between the two plates. The thin line with the stars represents the difference of the local energies. In the insert: Rectangular plates with high damping excited with a random white noise at point  $s_1$ . The spring is successively attached to 108 points along the line  $d_1$ . (b) Relative error between the coupling coefficient predicted theoretically with Eq. (3) and numerically with Eq. (10).

379 The excitation signal is a white noise with a cut-off frequency of 7 MHz generated via a  
380 Agilent 33210A signal generator. The signal is then filtered with an SR650 bandpass filter  
381 between 10 Hz and 8 kHz and amplified by a Brüel & Kjaer power amplifier type 2718. This  
382 filtered signal drives a shaker Brüel & Kjaer type 4810 which applies a transverse force to  
383 plate 1.

384 Two accelerometers PCB 352C67 are attached with wax to the two plates at the position  
385 of the spring attachment but on the opposite side. These accelerometers have a sensitivity of  
386 100 mV/g and allow measurements from 0.5 Hz to 10 kHz. The mass of these accelerometers  
387 is 2 g which is negligible compared to the mass of the plate which is 2 kg. To measure  
388 the force injected into the system, a Brüel & Kjaer impedance head type 8001 is screwed  
389 on the shaker. The impedance head is connected to a Brüel & Kjaer type 2635 charge  
390 amplifier. The data acquisition is done with a National Instruments NI 9234 acquisition  
391 board with a sampling frequency of 12.8 kHz per channel. The averaging is performed with  
392 20 measurements with an overlap factor of 25 % representing an acquisition time of 25.6 s.  
393 A Hamming window is applied to each measurement. With the software M+P Analyzer, the  
394 time signal is processed and the frequency response function is obtained with the estimator  
395  $H_2$ .

396 To ensure that the energy is transmitted only through the coupling spring and not through  
397 the frame, the spring is first disconnected plate 1 being always excited. The energy of plate  
398 2 without the coupling is found 35 dB less than with the coupling. This gives the part of  
399 energy transmitted through the frame or the air.

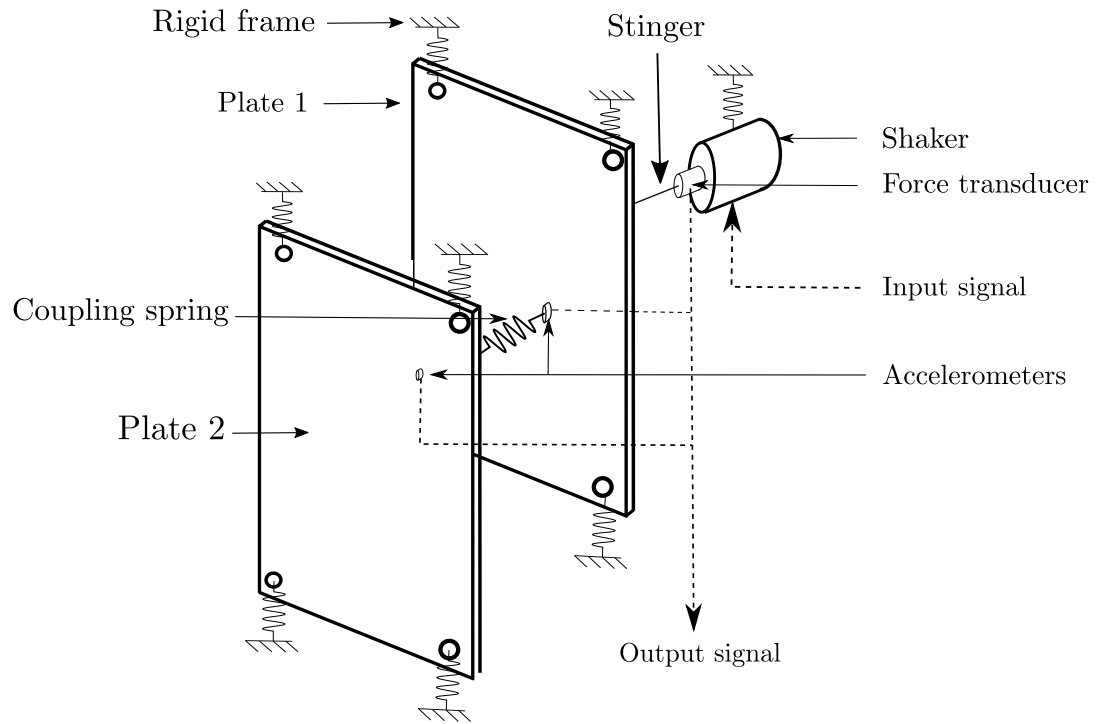


FIG. 12. Experimental set-up. Both plate 1 and 2 are coupled with a spring. The shaker excites plate 1 through the stinger, which is bonded to the plate. The force injected is measured with a force transducer. The acceleration of both plates is measured at the coupling point with the accelerometers.

#### 400 **B. Measurement protocol**

401 The different steps performed to measure the plate energy, the power exchanged and the  
 402 coupling coefficient are the followings. The excitation is located at point  $\mathbf{s}_0$  ( $x= 0.12$  m;

403  $y=0.2$  m). The origin of the reference frame is the centre of the plate. The coordinates  
 404 of the different measurements and coupling points are presented in Table II.  $\mathbf{s}_1$  and  $\mathbf{s}_2$  are  
 405 points with an energy enhancement equal to  $9/4$ ,  $\mathbf{d}_1$ ,  $\mathbf{d}_2$  and  $\mathbf{d}_3$  are points with an energy  
 406 enhancement of  $3/2$ .

TABLE II. Attachment points of spring on plate 1 (m).

$\mathbf{s}_1$	$\mathbf{s}_2$	$\mathbf{d}_1$	$\mathbf{d}_2$	$\mathbf{d}_3$	1	2	3
(0.1; 0,5)	(0.1; 0.1)	(0.1; 0.35)	(0.22; 0.5)	(0.1; 0.25)	(0.25; 0.35)	(0.2; 0.25)	(0.25; 0.2)

407 For each attachment point of the spring, the measurements are performed five times and  
 408 the average is calculated. Between each measurement the two accelerometers are taken off  
 409 and then put back at the same point. A slight variation in measurement is observed due  
 410 to the thickness of the wax and the slight variation in the measurement position. In order  
 411 to quantify this uncertainty, 100 measurements are made for measurement point 1 and the  
 412 standard deviation is calculated and is equal to 0.71 dB.

413 From accelerometers measurements, the local energy at the coupling points  $e_1^{exp}$  and the  
 414 exchanged power  $P^{exp}$  are calculated. Finally the coupling coefficient is calculated with

$$\beta^{exp} = \frac{P^{exp}}{e_1^{exp}(\mathbf{r}_1)A_1/n_1 - e_2^{exp}(\mathbf{r}_2)A_2/n_2}. \quad (11)$$

415 with  $A_i$  the surface of the plate and  $n_i$  the modal densities of the plate  $i$  determined numer-  
 416 ically.

417 **C. Results**

418 The experimental results with two coupled rectangular plates are shown in Fig. 13(a).  
 419 Fig. 13(a) shows the difference in local energies at the coupling point  $e_1^{exp}(\mathbf{r}_1)A_1/n_1 -$   
 420  $e_2^{exp}(\mathbf{r}_2)A_2/n_2$  and the exchanged power  $P^{exp}$ . Looking at Fig. 13(a), we see that the lines  
 421 and the points with energy enhancement appear well because the energy on the lines ( $\mathbf{d}_i$ )  
 422 and on the points ( $\mathbf{s}_i$ ) is higher than the energy on the rest of the plate. These experimental  
 423 enhancement factors are very close to the theoretical values. Moreover, the exchanged power  
 424 evolves in a proportional way to the difference of the local energies.

425 Fig. 13(b) presents the relative error between the experimental coupling coefficient and  
 426 the coupling coefficient  $\beta$  given in Eq. (3). The two values agree well and the average error  
 427 is equal to 25.2%. This validates experimentally for this case the proposed Eq. (5) in cases  
 428 of inhomogeneous vibrational fields.

429 **VI. THERMODYNAMIC INTERPRETATION**

430 In statistical energy analysis, we use the modal energy  $E/N$  where  $N = n\Delta\omega$  is the  
 431 number of resonant modes in the frequency band  $\Delta\omega$  and  $E$  the total vibrational energy  
 432 of the subsystem. The subsystem is assumed to be in equilibrium in the sense that the  
 433 energy  $E$  is equally shared between a large number of modes  $N$ . In thermodynamics, the  
 434 temperature is defined for a system at equilibrium (all points of the system have the same  
 435 energy) as the total energy divided by the number of molecules (or atoms or degrees of

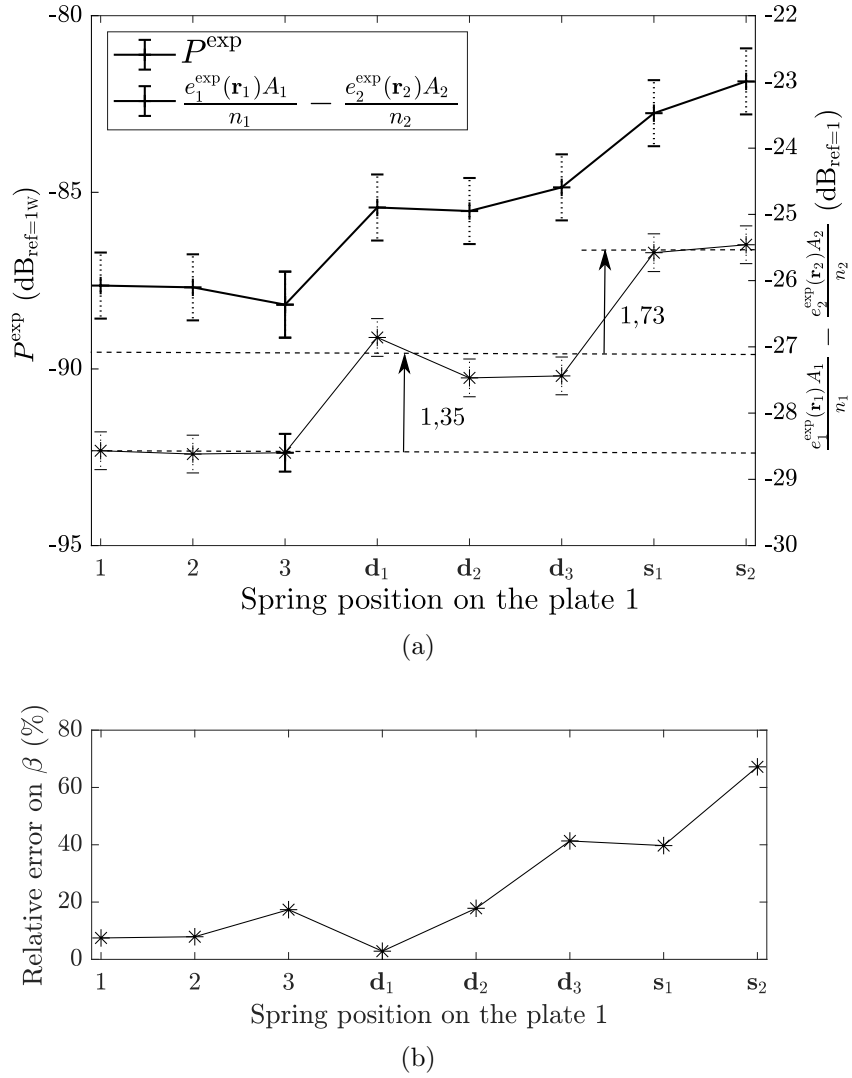


FIG. 13. (a) Comparison between the exchanged powers and the difference of the local energies obtained experimentally. (b) Relative error between the theoretical ( $\beta^{\text{th}}$ ) and the experimental ( $\beta^{\text{exp}}$ ) coupling coefficient.

436 freedom). It is rather common in SEA literature<sup>35</sup> to define the vibrational temperature as

$$T = \frac{E}{k_B N} \quad (12)$$

437 where  $k_B$  is Boltzmann's constant. But,  $E = eA$  where  $e$  is the energy density and  $A$  the  
 438 system area, and  $N = A\omega\Delta\omega/2\pi c_p c_g$  with  $c_p$  and  $c_g$  the group and phase velocities. The ratio

439  $E/N$  no longer depends on the area and is therefore a local quantity. It may be interpreted  
 440 as the local vibrational temperature. When the system is no longer in equilibrium (or when  
 441 the vibrational field is no longer diffuse), Eq. (5) reads

$$P = \beta k_B \Delta \omega (T_1 - T_2). \quad (13)$$

442 where now  $T_1$  and  $T_2$  are the local vibrational temperatures at the exchange point. It is now  
 443 apparent that Eq. (13) states that the power transmitted from subsystem 1 to subsystem 2 is  
 444 proportional to the difference of local temperatures similarly to the thermal conduction. The  
 445 coupling power proportionality is similar to Clausius' principle which states that thermal  
 446 energy always flows from high temperature to low temperature.

## 447 VII. CONCLUSION

448 In this paper, we have highlighted that the requirement of diffuse field in statistical energy  
 449 analysis may be by-passed provided that the local energies are known at the coupling points.  
 450 The key result is that a local form of the coupling power proportionality turns out to remain  
 451 valid even at points where the local energy is not equal to the spatial average of energy.

452 In order to reach this result, four different systems have been studied with mainly three  
 453 causes of non-diffuseness. First, spatial symmetries induce energy enhancement by coherence  
 454 of rays at some particular lines or points (lightly damped rectangular plate or stadium).  
 455 Second, non-ergodicity may induce a heterogeneity of field due to the presence of caustics  
 456 (circular plate). Third, high damping frustrates the homogeneity of field by imposing a  
 457 domination of the direct field (highly damped rectangular plate).

458 Of course, this result does not presume the way by which the information of local energy  
 459 is obtained. Within the framework of a strict application of statistical energy analysis, this  
 460 seems to be out of range. However, direct measurements of local energy or application of  
 461 theoretical enhancement factors can offer insights to improve the predictability of statistical  
 462 energy analysis. In all other cases, it might also be possible to implement more advanced  
 463 theories such as ray-tracing or geometrical theory of diffraction for predicting interference  
 464 effects, dynamical energy analysis or radiative energy transfer to account for non homo-  
 465 geneity in wave propagation, statistical modal energy distribution analysis for non uniform  
 466 modal distribution, or even any other theory capable of delivering an information on the  
 467 distribution of vibrational energy.

## 468 **APPENDIX A: CALCULATION OF RECEPTANCE**

469 The calculation of the receptance  $H$  of the coupled plates used in equations (6) and (9)  
 470 is presented in this Appendix.

471 The coupling spring of stiffness  $K$  is attached at points  $\mathbf{r}_1$  on plate 1 and  $\mathbf{r}_2$  on plate 2.  
 472 A unit harmonic force  $\exp(i\omega t)$  is applied to plate 1 at  $\mathbf{s}$  as shown in Fig. 1. We denote by  
 473  $H(\mathbf{r}, \mathbf{s}; \omega)$  the receptance of the coupled plates with a receiver at  $\mathbf{r}$  in plate 1 or 2 and a unit  
 474 harmonic force at point  $\mathbf{s}$  in plate 1. We also denote by  $H_i(\mathbf{r}, \mathbf{s}; \omega)$  the receptance of plate  $i$   
 475 isolated from the other plate.

476 Plate 1 is submitted to two forces: the external force  $F = 1$  applied at  $\mathbf{s}$  and the force  
 477  $K(u_2(\mathbf{r}_2) - u_1(\mathbf{r}_1))$  exerted by the spring at  $\mathbf{r}_1$ . The receptance  $H$  at any receiver  $\mathbf{r}$  in plate

478 1 is therefore

$$H(\mathbf{r}, \mathbf{s}; \omega) = H_1(\mathbf{r}, \mathbf{s}; \omega) + K(u_2(\mathbf{r}_2) - u_1(\mathbf{r}_1))H_1(\mathbf{r}, \mathbf{r}_1; \omega); \quad (\text{A1})$$

479 Plate 2 is excited by only one force, the spring reaction at point  $\mathbf{r}_2$ . The receptance  $H$  at  
 480 any receiver in plate 2 is therefore

$$H(\mathbf{r}, \mathbf{s}; \omega) = -K(u_2(\mathbf{r}_2) - u_1(\mathbf{r}_1))H_2(\mathbf{r}, \mathbf{r}_2; \omega) \quad (\text{A2})$$

481 But the receptance  $H$  at  $\mathbf{r}_1$  is the deflection  $u_1(\mathbf{r}_1)$  and at  $\mathbf{r}_2$  the deflection  $u_2(\mathbf{r}_2)$ .

482 Substituting  $\mathbf{r} = \mathbf{r}_1$  in equation (A1) and  $\mathbf{r} = \mathbf{r}_2$  in equation (A2) gives

$$\begin{aligned} u_1(\mathbf{r}_1) &= H_1(\mathbf{r}_1, \mathbf{s}; \omega) + K(u_2(\mathbf{r}_2) - u_1(\mathbf{r}_1))H_1(\mathbf{r}_1, \mathbf{r}_1; \omega); \\ u_2(\mathbf{r}_2) &= -K(u_2(\mathbf{r}_2) - u_1(\mathbf{r}_1))H_2(\mathbf{r}_2, \mathbf{r}_2; \omega) \end{aligned} \quad (\text{A3})$$

483 This gives a set of two linear equations on the unknowns  $u_1(\mathbf{r}_1)$  and  $u_2(\mathbf{r}_2)$ . Then, the  
 484 receptance  $H$  is obtained with equations (A1) and (A2).

485 **References**

486 <sup>1</sup>R. H. Lyon and G. Maidanik, “Power flow between linearly coupled oscillators,” J. Acoust.  
487 Soc. Am. **34**(5), 623–639 (1962).

488 <sup>2</sup>D. Newland, “Calculation of power flow between coupled oscillators,” J. Sound Vib. **3**(3),  
489 262–276 (1966).

490 <sup>3</sup>D. Newland, “Power flow between a class of coupled oscillators,” J. Acoust. Soc. Am.  
491 **43**(3), 553–559 (1968).

492 <sup>4</sup>T. D. Scharton and R. H. Lyon, “Power flow and energy sharing in random vibration,” J.  
493 Acoust. Soc. Am. **43**(6), 1332–1343 (1968).

494 <sup>5</sup>A. Le Bot, *Foundation of statistical energy analysis in vibroacoustics* (Oxford University  
495 Press, 2015).

496 <sup>6</sup>A. Le Bot, A. Carcaterra, and D. Mazuyer, “Statistical vibroacoustics and entropy con-  
497 cept,” Entropy **12**(12), 2418–2435 (2010).

498 <sup>7</sup>R. L. Weaver, “Diffuse waves in finite plates,” J. Sound Vib. **94**(3), 319–335 (1984).

499 <sup>8</sup>R. H. Lyon, “Needed: a new definition of diffusion,” J. Acoust. Soc. Am. **56**(4), 1300–1302  
500 (1974).

501 <sup>9</sup>L. Maxit and J.-L. Guyader, “Extension of sea model to subsystems with non-uniform  
502 modal energy distribution,” J. Sound Vib. **265**(2), 337–358 (2003).

503 <sup>10</sup>G. Zhu, L. Maxit, N. Totaro, and A. Le Bot, “A hybrid modal/statistical formulation for  
504 predicting the energy response of vibroacoustic systems in the mid frequency range,” J.  
505 Sound Vib. **538**, 117221 (2022).

506 <sup>11</sup>A. Le Bot, “A vibroacoustic model for high frequency analysis,” J. Sound Vib. **211**, 537–  
507 554 (1998).

508 <sup>12</sup>A. Le Bot and A. Bocquillet, “Comparison of an integral equation on energy and the  
509 ray-tracing technique in room acoustics,” J. Acoust. Soc. Am. **108**, 1732–1740 (2000).

510 <sup>13</sup>A. Le Bot, “Energy transfer for high frequencies in built-up structures,” J. Sound Vib.  
511 **250**, 247–275 (2002).

512 <sup>14</sup>A. Le Bot and E. Sadoulet-Reboul, “High frequency vibroacoustics: A radiative transfer  
513 equation and radiosity based approach,” Wave Motion **51**(4), 598–605 (2014).

514 <sup>15</sup>G. Tanner, “Dynamical energy analysis-determining wave energy distributions in vibro-  
515 acoustical structures in the high frequency regime,” J. Sound Vib. **320**, 1023–1038 (2009).

516 <sup>16</sup>G. Tanner and S. Giani, “Wave transport in complex vibro-acoustic structures in the high-  
517 frequency limit,” in *Symposium on the vibration analysis of structures with uncertainties*,  
518 edited by A. K. Belyaev and R. Langley, Springer (2011), pp. 187–200.

519 <sup>17</sup>T. Hartmann, S. Morita, G. Tanner, and D. Chappell, “High frequency structure- and  
520 air-borne sound transmission for a tractor model using dynamical energy analysis,” Wave  
521 Motion **87**, 132–150 (2019).

522 <sup>18</sup>A. Le Bot, “Derivation of statistical energy analysis from radiative exchanges,” J. Sound  
523 Vib. **300**(3-5), 763–779 (2007).

524 <sup>19</sup>B. Mace, “Power flow between two continuous one-dimensional subsystems: a wave solu-  
525 tion,” J. Sound Vib. **154**(2), 289–319 (1992).

- 526 <sup>20</sup>G. Maidanik and J. Dickey, “Wave derivation of the energetics of driven coupled one-  
527 dimensional dynamic systems,” *J. Sound Vib.* **139**(1), 31–42 (1990).
- 528 <sup>21</sup>R. Lyon and E. Eichler, “Random vibration of connected structures,” *J. Acoust. Soc. Am.*  
529 **36**, 1344–54 (1964).
- 530 <sup>22</sup>W. Wöhle, T. Beckmann, and H. Schreckenbach, “Coupling loss factors for statistical  
531 energy analysis of sound transmission at rectangular structural slab joints, part i,” *J.*  
532 *Sound Vib.* **77**(3), 323–334 (1981).
- 533 <sup>23</sup>K. Itao and S. Crandall, “Wide-band random vibration of circular plates,” *Transactions*  
534 *of the ASME* **100**, 690–695 (1978).
- 535 <sup>24</sup>A. Langley and P. Taylor, “Chladni patterns in random vibration,” *International Journal*  
536 *of Engineering Science* **17**(9), 1039–1047 (1979).
- 537 <sup>25</sup>A. Le Bot, O. Robin, K. Rouard, and A. Berry, “Analysis of random mechanical vibrations  
538 in symmetrical thin plates using full-field vibration measurements,” *Journal of Vibration*  
539 *and Acoustics* **143**(2), 024503 (2021).
- 540 <sup>26</sup>V. Tyrode, N. Totaro, L. Maxit, and A. Le Bot, “Coherent wave reflection in integrable or  
541 chaotic symmetrical acoustical billiards,” *Proceedings of the Royal Society A* **477**(2255),  
542 20210488 (2021).
- 543 <sup>27</sup>T. Lafont, N. Totaro, and A. Le Bot, “Review of statistical energy analysis hypotheses in  
544 vibroacoustics,” *Proc. R. Soc. A* **470**(2162), 20130515 (2014).
- 545 <sup>28</sup>T. Lafont, N. Totaro, and A. Le Bot, “Coupling strength assumption in statistical energy  
546 analysis,” *Proc. R. Soc. A* **470**(2162), 20130515 (2017).

547 <sup>29</sup>A. Keane and W. Price, “Statistical energy analysis of strongly coupled systems,” *J. Sound*  
548 *Vib.* **117**(2), 363–386 (1987).

549 <sup>30</sup>F. Fahy and Y. de Yuan, “Power flow between non-conservatively coupled oscillators,” *J.*  
550 *Sound Vib.* **114**, 1–11 (1987).

551 <sup>31</sup>A. Le Bot and V. Cotoni, “Validity diagrams of statistical energy analysis,” *J. Sound Vib.*  
552 **329**(2), 221–235 (2010).

553 <sup>32</sup>A. Le Bot, Z. Bazari, P. Klein, and J. Lelong, “Statistical analysis of vibration in tyres,”  
554 *J. Sound Vib.* **392**, 187–199 (2017).

555 <sup>33</sup>H. Li, N. Totaro, L. Maxit, and A. Le Bot, “Ergodic billiard and statistical energy analy-  
556 sis,” *Wave Motion* **87**, 166–178 (2019).

557 <sup>34</sup>G. Tanner and N. Søndergaard, “Wave chaos in acoustics and elasticity,” *J. Phys. A: Math.*  
558 *Theor.* **40**(50), R443–R509 (2007).

559 <sup>35</sup>A. Le Bot, “Entropy in statistical energy analysis,” *J. Acoust. Soc. Am.* **125**(3), 1473–1478  
560 (2009).